



Aeropropulsive Interaction and Thermal System Integration within the ECO-150: A Turboelectric Distributed Propulsion Airliner with Conventional Electric Machines

Benjamin T. Schiltgen¹, Jeffrey L. Freeman²

Empirical Systems Aerospace, Inc., Pismo Beach, CA, 93448

and

David W. Hall³

DHC Consulting, Foster City, CA, 94404

The ECO-150 is a 150 passenger Environmentally CONscious tube-and-wing regional airliner concept which is characterized by a turboelectric distributed propulsion (TeDP) system embedded within the inboard section of the wing. Since 2008, the ECO-150 concept has served to promote a more complete understanding of TeDP performance, integration, design requirements, and system complexities. Early versions of the ECO-150 claimed superconducting electronics cooled by onboard liquid hydrogen (LH_2); however, the infrastructure requirements of such a system are far out of reach for near-term technology. In this most recent investigation, the ECO-150R was equipped with conventional electric machines suitable for NASA's N+2 timeframe. A recirculating liquid thermal management system (TMS) with ram air heat exchangers was integrated into the design to support the electric machines. Additionally, three-dimensional CFD analysis of the aircraft guided a redesign of the inboard wing and validated prior lower-order estimates for aero-propulsive efficiency and high lift performance. Component integration exercises within the updated configuration illuminated unexpected yet solvable packaging challenges. Mission performance analysis showed the ECO-150R concept to be at least as efficient as a currently operating airliner despite systematically conservative assumptions for the mass and efficiency of the advanced technologies and several unclaimed opportunities for design optimization. Ultimately, the research discussed in this paper strengthened the credibility of the ECO-150 concept and confirmed the feasibility of TeDP systems with conventional electric machines.

Nomenclature

| | |
|------------|--|
| C_L | = coefficient of lift |
| C_P | = coefficient of pressure |
| D | = aircraft total drag, lb_f |
| L | = aircraft total lift, lb_f |
| M | = Mach number |
| T | = aircraft total thrust, lb_f |
| $TOFL$ | = takeoff field length, ft |
| $TSFC$ | = thrust specific fuel consumption, $lb_m/lb_f/hr$ |
| ΔT | = difference in temperature, $^{\circ}R$ |

¹ VP of Finance / Aerospace Engineer, P.O. Box 595, Pismo Beach, CA, Senior Member

² Aerospace Engineer, P.O. Box 595, Pismo Beach, CA, Professional Member

³ 1288 East Hillside Boulevard, Apartment B-110, Foster City, CA, 94404, AIAA Lifetime Associate Fellow

I. Introduction

Empirical Systems Aerospace, Inc. (ESAero) has been performing design studies of advanced aircraft that utilize turbo-electric distributed propulsion (TeDP) and the more generic hybrid-electric distributed propulsion (HEDP), and developing methodologies and tools for them since 2008, starting with the ECO-150-16 (Figure 1). These vehicles require new high specific power and increased efficiency, meaning superconducting components for transports may be beneficial. Previous work included propulsion system design and analysis in concert with complete aircraft system design and performance estimation¹⁻³. Both cryogenically-cooled and non-cryogenically cooled systems have been considered across multiple projects with multiple customers, both government and private. ESAero recently concluded a redesign effort of the ECO-150 to exercise newly developed design tools and improve credibility of the split-wing concept; this effort produced the ECO-150R⁴.

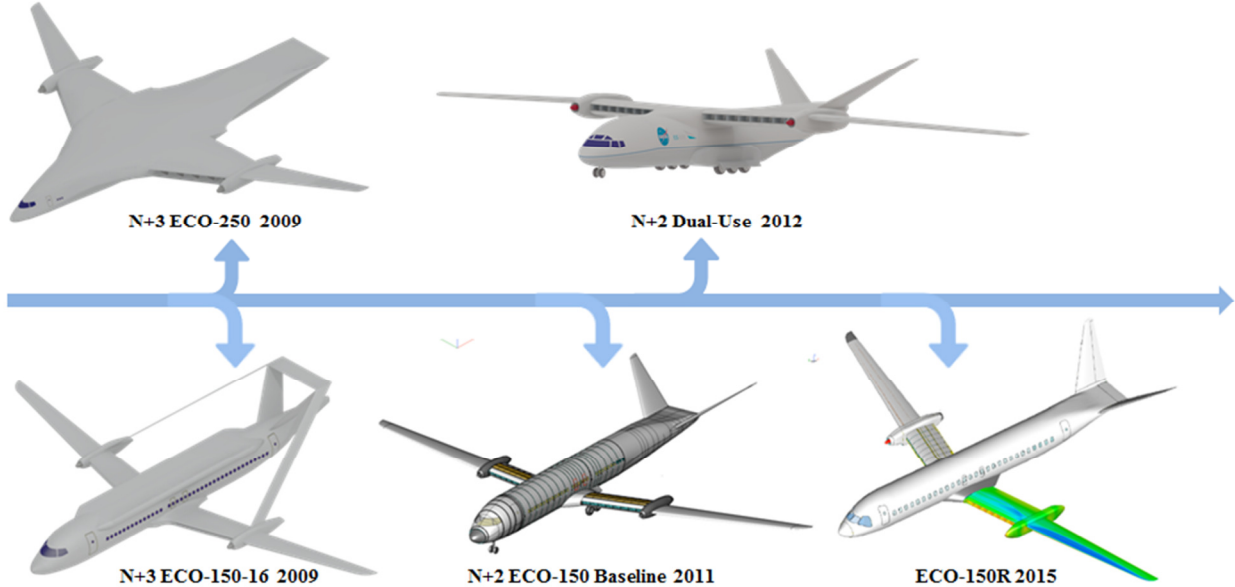


Figure 1. ECO Configuration Genealogy; Left to Right; Original SBIR Superconducting ECO-150-16 and ECO-250, NASA ERA N+2 ECO-150 Baseline, AFRL/NASA Conventional “Warm” Machine Dual-Use, Revised Conventional Machine ECO-150R.

The ECO-150-16 and ECO-250, both shown in Figure 1, were designed during ESAero's first NASA SBIR in 2009¹. Each side of the split-wing carries an outboard turboshaft engine and generator which powers an array of “*N*” electrically-driven, embedded fans along with other on-board electrical devices. The tube-and-wing ECO-150-16 was a promising concept that showed a 40% reduction in fuel burn from which many of ESAero's future efforts evolved; this vehicle is still being used by ESAero and NASA as a potential configuration and is undergoing NASA review as part of the Advanced Air Transportation Technologies (AATT) project. The hybrid-wing body ECO-250 was less promising, only achieving a 5% reduction in fuel burn. Both of these vehicles carried large liquid hydrogen (LH_2) tanks which were used to regulate the temperature of the high power superconducting electronics. Battery power supplementation was not considered for either of these aircraft.

In the following year, 2010, ESAero was awarded a follow-on NASA SBIR to further develop the Integration of a Distributed Fan Propulsion (IDFP) concept using the ECO-150-16 as the baseline vehicle².

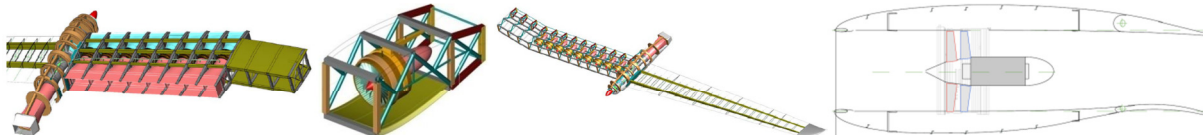


Figure 2. ECO-150 split-wing truss structure with embedded fans.

Under this contract, the split-wing concept with the propulsors mounted inside the wing, shown in Figure 2, was studied to determine its effect on wing structure, propulsor performance, and overall wing aerodynamics. The inboard wing section's truss-frame structure was found to be inherently stiff, and the study showed that later

renditions of the split-wing concept did not require compression strut braces and could credit a 22% reduction in wing weight as compared to conventional wings of similar planform.

In 2011, ESAero performed a NASA Environmentally Responsible Aircraft (ERA) investigation to redesign the ECO-150 and develop a Dual-Use Commercial/Military high-winged transport for NASA Ames and AFRL, both of which would utilize conventional electric components rather than cryogenically cooled machines³. The goal of this study was to determine if HEDP configurations could be feasible in the N+2 timeframe without relying on cryogenic technology. These vehicles utilized turbogenerators with battery supplementation while maintaining the split-wing design from the ECO-150-16. Among the components considered during this study are turboshaft engines, electrical generators and motors, electrical power management (i.e. transformers, inverters, etc.), power distribution cables and busses, electrical machine controllers, and ducted fans. Although the projected fuel savings of these N+2 designs was worse than for the superconducting ECO-150-16, the study showed that aircraft designs with HEDP systems could close.

It was the overall objective of the most recent effort to address new aerodynamic concepts, propulsion systems, thermal management systems, propulsion-airframe-thermal integration (PATI) and the overall integration into the ECO-150 for the 2030-2040 time frame by leveraging significant advancements over the previous 7 years. The specific objectives of this effort were three-fold:

1. Solidify the potential of electric propulsion systems for subsonic transport aircraft to meet the vehicle efficiency, fuel burn and safety requirements established by the NASA by re-configuring the ECO-150 using the latest design methodologies and capabilities.
2. Establish a roadmap for the sizing and synthesis of propulsion system and thermal management system (TMS) components within TeDP and HEDP architectures.
3. Incorporate the results/lessons learned from the recent AFRL propulsion-airframe integration (PAI) studies⁵. Conduct similar CFD analysis to verify the aerodynamic assumptions for the ECO-150 split wing, and feed those results back directly into the conceptual re-design process.

The pursuit of these objectives and the latest model of the ECO aircraft line, the ECO-150R, are presented in this paper.

II. Propulsion System Sizing

A custom design and analysis software named PANTHER (Propulsion Airframe iNTegration for Hybrid Electric Research) was used to design the propulsion system in the ECO-150R. PANTHER has been progressively developed through a variety of NASA SBIR contracts beginning in 2013^{6-8,4}. A logic flow diagram for PANTHER which highlights recent additions is shown in Figure 3. The algorithm consists of a primary iteration loop that converges on vehicle mass and operating behavior. The components modeled in PANTHER are characterized by a toolbox of empirical and physics-based component sizing and performance analysis subroutines. Many of the subroutines were originally developed for HAPSS (Hybrid Aircraft Propulsion System Synthesis)^{9,10}. A pass through the iteration loop begins with a prediction of thrust requirements for each propulsor at every design condition^{11,12}. PANTHER traces this component-specific performance requirement “upstream” (i.e. against the flow of power) through the powertrain, sizing and evaluating the performance of each component along the way. Propulsion system components considered for the ECO-

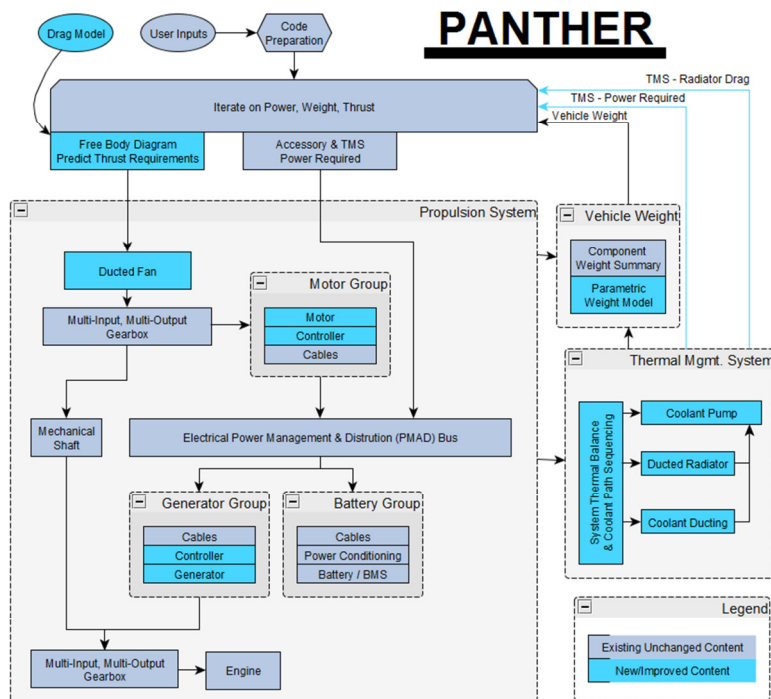


Figure 3. PANTHER On-Design Mode Logic Flow Diagram.

150R include ducted fans, gearboxes, motors/generators and their controllers, high ampacity power cables and turboshaft engines. A power management and distribution (PMAD) bus architecture was used to transmit the power produced by the engines to all of the propulsors. After the propulsion system portion of the iteration loop is completed, a thermal management system (TMS) is sized to regulate the temperature of the electronics and reject heat from the aircraft. The TMS included coolant reservoirs, pumps, plumbing, and ram air heat exchangers. Finally, a parametric weight model is used to update the vehicle's weight, which results in revised requirements for lift, drag, and thrust; thus the iteration cycle begins again, continuing until convergence.

The propulsion system architecture for the ECO-150R was influenced by a study performed by Rolls-Royce which showed that symmetric thrust distribution can be maintained in the event of an engine or fan failure with a properly designed electric microgrid¹³. This practice can diminish the design impact of off-nominal conditions on power transmission components and the vertical tail. The dual inner bus tie power distribution architecture shown in Figure 4 is a relatively simple architecture which allows full power from one engine to be equally distributed to all fans if the other engine fails. Each of the four DC buses powers four propulsion units which are arranged to negate the yaw impact of a bus failure. This architecture is a slight extrapolation of the Inner Bus Tie concept presented in Ref. 13. Future research on this topic should include weight and efficiency influences of power circuit protection schema and quantitative tradeoff analysis between vertical tail sizing and PMAD design. For example, it is worth considering whether the weight added by routing power cables from one wing to the other pays for the improvements in vertical tail weight and drag.

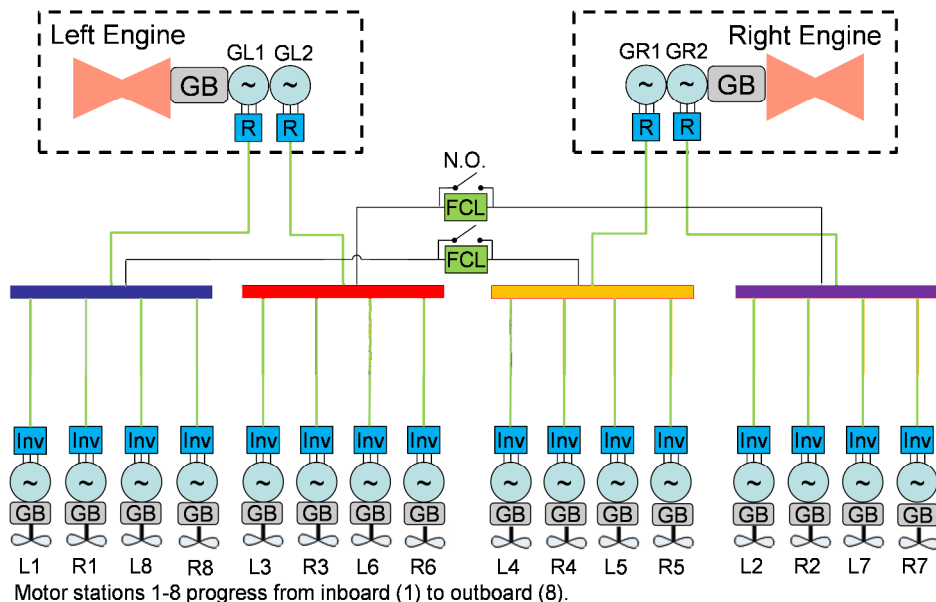


Figure 4. Dual Inner Bus Tie Electrical Power Distribution Architecture.

The flight conditions which were used to design the ECO-150R are listed in Table 1. Top of climb (TOC) is a common design-driving requirement for engines and air-breathing propulsors because of the low air density. Conversely, electrical components in the powertrain do not lapse with altitude and their performance requirements may be dominated by a low altitude maneuver. The one engine inoperable (OEI) climbout condition stipulates that one of the two turboshaft engines is inoperable but, thanks to the electrical PMAD bus, all of the remaining engine's power can be equally distributed to all sixteen operational fans.

Table 1. Design Conditions for the ECO-150R.

| | Top of Climb | Takeoff | OEI Climbout | Cruise (OD) |
|------------------------------|--------------|-------------|--------------|--------------|
| Mach Number | 0.65 | 0.2 | 0.2 | 0.7 |
| Altitude, ft | 30000 | 0 | 0 | 30000 |
| ΔT from ISA Std., 'R | 0 | 0 | 0 | 0 |
| Weight Fraction | 0.92 | 1 | 1 | 0.92 |
| Sp. Excess Power, ft/min | 500 | n/a | n/a | 0 |
| TOFL, ft | n/a | 5000 | n/a | n/a |
| Object Height, ft | n/a | 50 | n/a | n/a |
| Climb Gradient, % | n/a | n/a | 2.4 | n/a |

The sizing criterion for each individual component in a TeDP architecture was brought into question. When an engine that is sized for TOC is at sea level, it may be capable of producing far more power than is required for all other design conditions, including OEI climbout. In such a scenario, should the subsequent components in the electrical powertrain (i.e. generators, converters, motors, etc.) be sized to harness all of the engine's available power? To do so could result in unnecessarily heavy powertrain components.

Although net thrust required at takeoff and OEI climbout are greater than is required for TOC, the thrust power is far greater at high speed. Therefore, the highest power demand for the motors, rectifiers, and load-side power cables is at TOC. In contrast, the loss of an engine in the OEI climbout condition results in far greater source-side power demand than is required during TOC; this influences sizing for generators, inverters, and source-side power cables. In both cases, the design driver for the components is carried upstream from the thrust requirement rather than downstream from engine power available. The source-side and load-side transmission components would need to be roughly 50% and 85% more powerful, respectively, to be able to harness the full power available by the two engines at sea level static (SLS) maximum power. It follows that each individual component should be designed to meet its particular performance requirements rather than unilaterally complying to support the power available from the engines. This approach allows each component to be critically sized to meet the design constraints. Figure 5 demonstrates the concept.

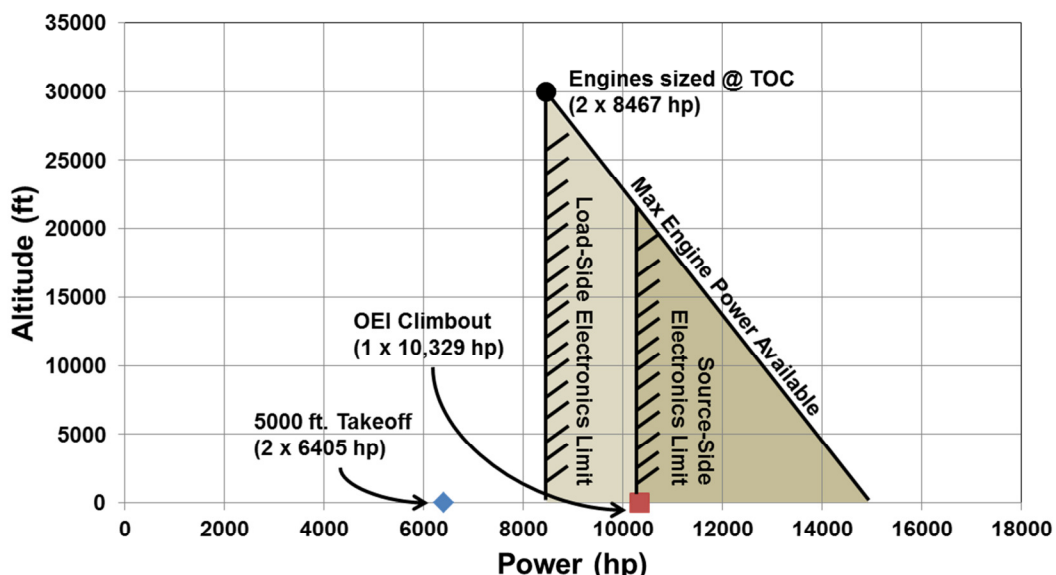
**Figure 5. Sizing Philosophy for ECO-150R Propulsion System Components.**

Figure 6 shows the ECO-150R's motor (a) and generator (b) efficiency maps with design condition operating points marked. The maps were scaled from typical performance of state-of-the-art machines, and a factor was added for future technology with higher efficiency. Gearboxes with 2:1 gear ratios were included in the powertrain to keep the motors and generators spinning appropriately slow for their diameters, however the inclusion of gearboxes should be reconsidered in the future with the support of physics-based electric machine design and analysis algorithms. It is interesting to note that the fans' preferred rotation speeds during the TOC and cruise conditions are much higher than those for the takeoff and OEI climbout conditions. It follows, then, that the motor torque at TOC is

lower than at takeoff even though TOC power is greater. In contrast, the generators are connected to a constant speed engine shaft and experience peak torque demand during OEI climbout.

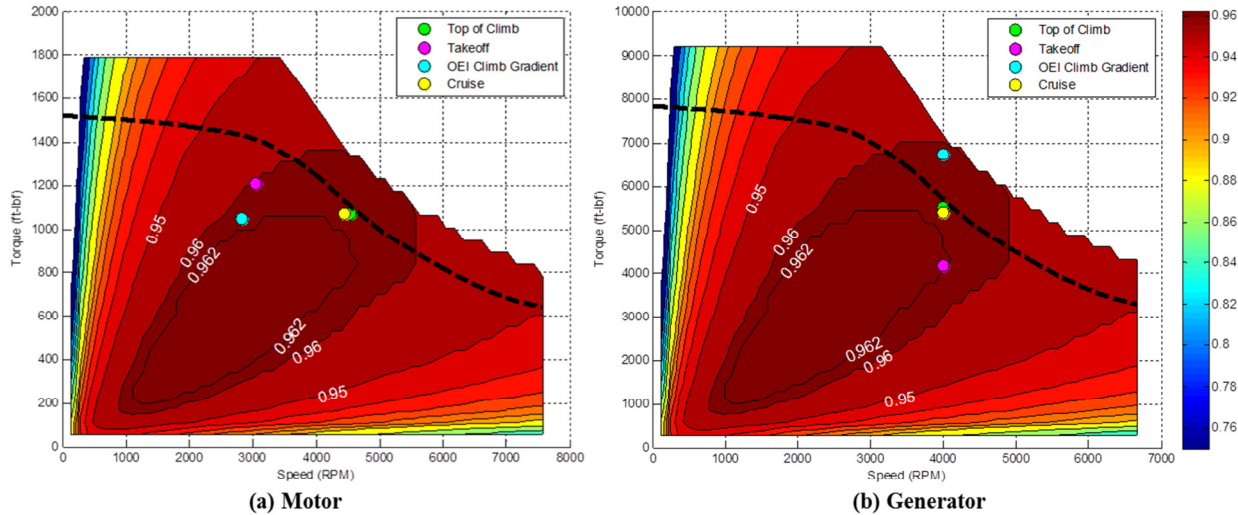


Figure 6. Operating Condition Placements on Motor and Generator Efficiency Maps.

Top-level results for the ECO-150R propulsion system are presented in Table 2. The propulsion group weight was found to be approximately one third of the vehicle empty weight. Cooling drag on the radiators is factored into the propulsion group performance as installation drag and effectively reduces the overall efficiency.

Table 2. Weights and Key Performance Indicators of the Propulsion Group.

| Propulsion Group Weight Total | 21017 | Key Performance Indicators | | | | |
|-------------------------------|-------|---------------------------------|-------|---------|-------|--------|
| Parametric Weight Models | | Flight Condition: | TOC | Takeoff | OEI | Cruise |
| Engine Controls | 949 | Net Thrust, lbf | 8865 | 12703 | 10276 | 8284 |
| Starting Systems | 258 | Net Thrust Power, hp | 10421 | 5157 | 4172 | 10487 |
| Upper Wing Thrust Reversers | 812 | Maneuver Thrust, lbf | 8646 | 12308 | 9885 | 8041 |
| Air Injection Ducts | 1390 | Installation Drag, lbf | 219 | 394 | 391 | 243 |
| PANTHER Details | | Net Fuel Flow, lbm/hr | 4671 | 5481 | 3648 | 4534 |
| Turboshaft Engines | 3304 | Average Power Supply Efficiency | 49.7% | 32.0% | 38.8% | 50.1% |
| Engine Gearboxes | 413 | Transmission Efficiency | 87.3% | 87.1% | 86.8% | 87.3% |
| Propulsor Gearboxes | 296 | Average Propulsor Efficiency | 88.1% | 74.5% | 71.1% | 87.8% |
| Generators | 3885 | Thermal Efficiency | 38.2% | 20.8% | 24.0% | 38.4% |
| Motors | 3474 | Propulsive Efficiency | 80.2% | 62.1% | 65.4% | 82.6% |
| Power Inverters/ Controller | 1398 | Overall Efficiency | 30.6% | 12.9% | 15.7% | 31.8% |
| Power Cables | 1284 | Installed Overall Efficiency | 29.9% | 12.5% | 15.1% | 30.8% |
| Fans | 1732 | TSFC, lbm/lbf/hr | 0.540 | 0.445 | 0.369 | 0.564 |
| Radiators (Dry) | 691 | | | | | |
| Coolant Ducts (Dry) | 173 | | | | | |
| Coolant Pumps (Dry) | 154 | | | | | |
| Coolant Reservoir (Dry) | 25 | | | | | |
| Coolant | 781 | | | | | |

*All weights in lb_m

Figure 7 shows a top-level comparison of the ECO-150R against other existing and projected propulsion system technologies. The assumptions used for the ECO-150R are conservative and several opportunities for improvement have not yet been investigated, suggesting that warm electric TeDP configurations suitable for the N+2 timeframe will likely continue to improve by a substantial degree. It is clear here that the estimation for engine core thermal efficiency was woefully pessimistic for a futuristic aircraft; the currently used model was a trend of empirical engine data without any future factors applied. Furthermore, a more rigorous ducted fan optimization study could likely increase the propulsive efficiency. Finally, the TeDP concept can enable more aggressive technologies that carry the potential to yield step-change improvements in either transmission or cycle efficiency, such as LH₂-cooled superconducting TeDP and battery supplemented HEDP.

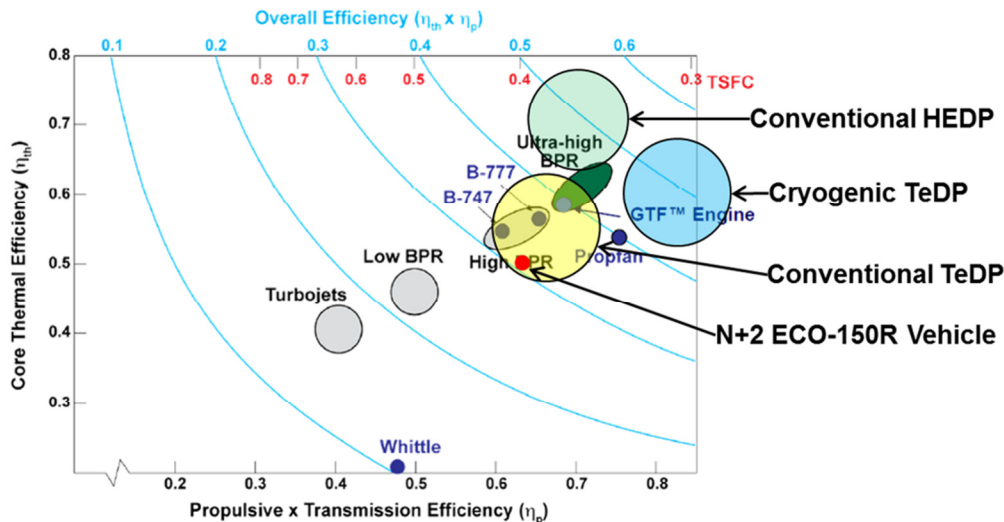


Figure 7. Propulsion System Overall Efficiency Comparison with TeDP and HEDP Projections. Modified from Ref. 14.

III. Thermal Management System Design and Sizing

Each electric component within the powertrain produces heat as a result of its inefficiency. Left unchecked, the component's operating temperature will increase until it exceeds its critical temperature and overheats. Therefore a thermal management system (TMS) must be designed to pull the heat away from each component and reject it from the aircraft. Due to the power levels involved in the ECO-150R, the electrical components are estimated to produce nearly 2000 hp (1491 kW) of heat at the top of climb flight condition. The motors and generators may experience some passive cooling depending on the design and integration of the machines, but that alone is not expected to be sufficient for thermal equilibrium.

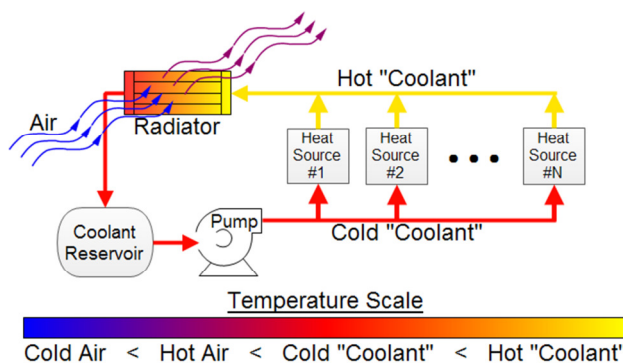


Figure 8. Thermal Management System Diagram.

fluids should be evaluated for this application.

The heat rejection capability of an aircraft is an often understated limiting factor on performance which can have a significant impact on the design of the vehicle¹⁵. For high speed applications, a feasible technology for continuous heat rejection is a ducted radiator. Made popular by the P-51 Mustang, ducted radiators are liquid-to-air heat exchangers ensconced in an air duct; they utilize the Meredith Effect¹⁶ to simultaneously increase heat rejection capacity and reduce cooling drag.

A physics-based ducted radiator sizing routine was established to support this investigation. The heat exchanger was assumed to be a simple tube-and-fin configuration with geometry parameters as presented in Figure 9. Additionally, the model supported analysis of multi-pass configurations wherein the coolant traverses back and forth across the airstream in a serpentine fashion. The heat transfer analysis was based on the prediction of thermal resistance¹⁷, and the heat exchanger effectiveness (ε) was calculated via the $\varepsilon - NTU$ approach assuming a mixed-

A recirculating liquid cooling system with ducted radiators (ram air heat exchangers) as the primary means of heat rejection was designed to support the ECO-150R electric transmission. A conceptual diagram of the TMS is shown in Figure 8. Two of these closed-loop systems are included on the aircraft—one for each half span. The heat sources consist of motors, generators, controllers, and power cables. This study has not considered the thermal requirements of the engines or gearboxes within the propulsion system as they are assumed to have a separate system. Furthermore, failure analysis and system redundancy of the TMS have yet to be addressed. Water was used as the coolant for the current study; however, designed coolant

air / unmixed-liquid crossflow arrangement¹⁸. Pressure loss for the coolant was determined using conventional pipe flow formulae. Inlet performance was estimated using a semi-empirical model which accounts for nominal diffuser pressure ratio, the augmented pressure ratio for takeoff and low speed conditions, and additive drag in high speed conditions¹⁹⁻²¹. Aerothermodynamics in the heat exchanger fin channels and in the nozzle were predicted via a general one-dimensional compressible flow algorithm which integrates the effects of area change, wall friction, and heat addition through the airstream²². Given geometry design details and operating design requirements, the sizing routine adjusts the radiator length—scaling heat exchanger face area and air mass flow rate accordingly—until the heat flow rate meets its target requirement.

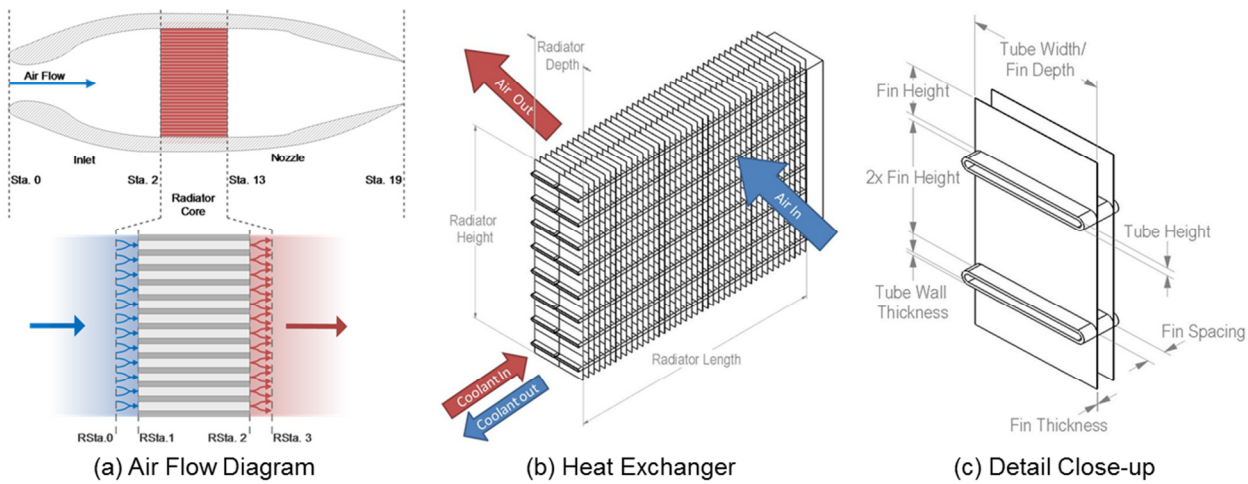


Figure 9. Tube-and-Fin Ducted Radiator.

Two parameters were identified to be of critical significance for the design and performance of the ducted radiator. The first critical parameter is the diffuser area ratio, defined as the ratio of cross-sectional areas at the inlet throat and the forward face of the heat exchanger (station 2). The second critical parameter is the Mach number at station 2 (a.k.a. face Mach), which can be independently controlled by a variable exit area nozzle. The amount of compression required to reduce the airspeed from the flight Mach number to the face Mach number is split between internal and external compression depending on these two parameters. The diffuser area ratio sets the amount of internal air compression whereas the remaining compression manifests as additive drag. The airflow within the duct was restricted to subsonic Mach numbers; parameter sets that violated this assumption were rejected. Furthermore, the pressure loss through the duct cannot be so extreme that it allows reverse flow in the nozzle.

A weighted multi-objective constrained optimizer was programmed to identify the values of diffuser area ratio and face Mach number which provide a balanced solution that is light weight while keeping cooling drag and the impact on pump power low. Figure 10 shows an on-design trade space evaluation for the ducted radiator at the top-of-climb design condition with the optimal solution marked by a green dot. It can be seen that the weight and pump power are closely related to the frontal face area of the heat exchanger, which is generally inversely proportional to face Mach. Although slower air passing through the heat exchanger improves its effectiveness, it ultimately reduces the heat transfer rate. The limiting constraint for the design occurred when the pressure loss through the duct was severe.

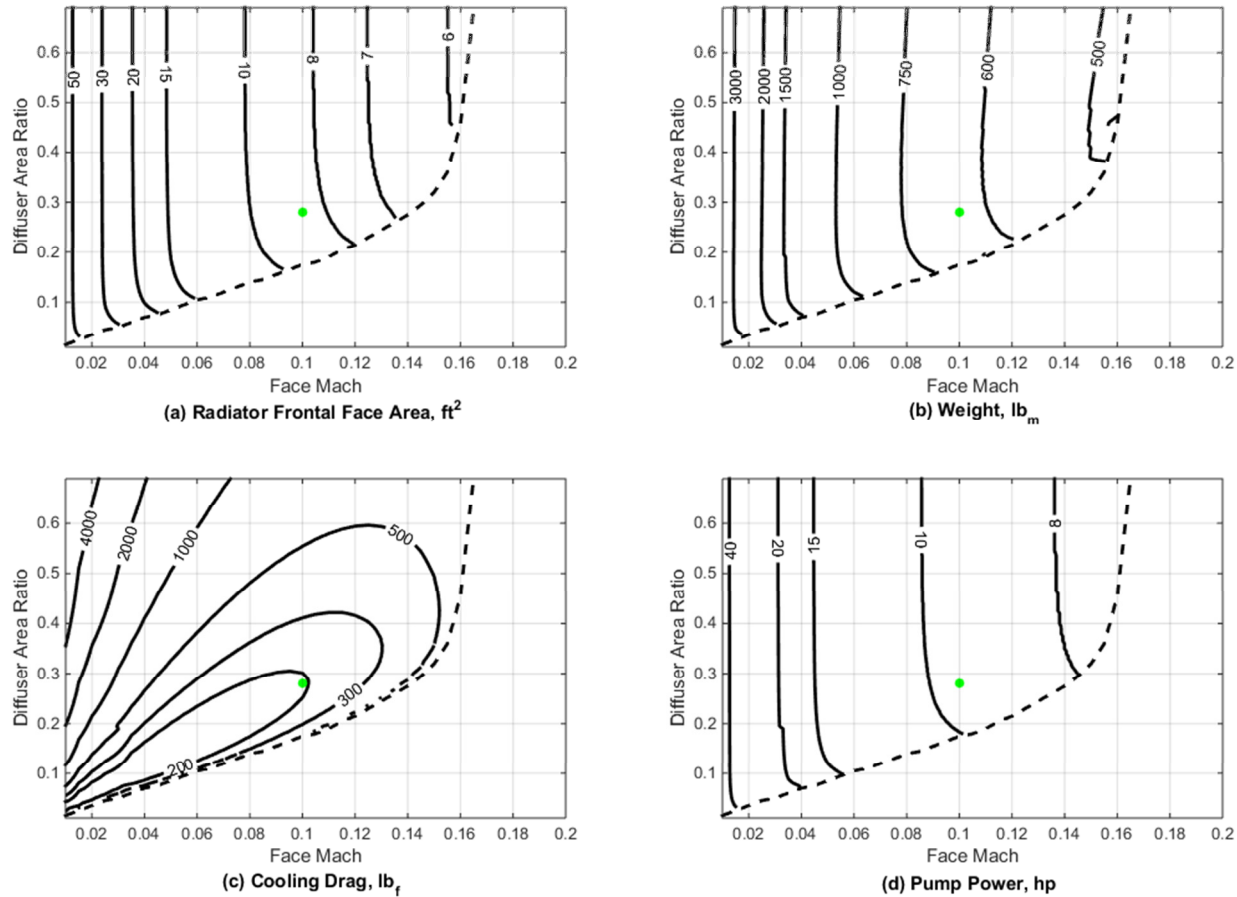


Figure 10. Ducted Radiator Top of Climb On-Design Trade Space with ECO-150R Solution Marked Green.

The chosen radiator design was then evaluated for off-design performance. During operation, the variable area nozzle exit can be controlled to achieve different results. It is typically desirable to minimize the drag caused by the ducted radiator while still expelling a sufficient amount of heat. Figure 11(a) shows a performance map for a system that is tuned for low drag. The black contours show the greatest heat flow possible with the low drag control tuning, and the red contours show the cooling drag associated with that condition. In extreme load circumstances, it may be preferable to increase the heat rejection rate at the expense of greater drag.

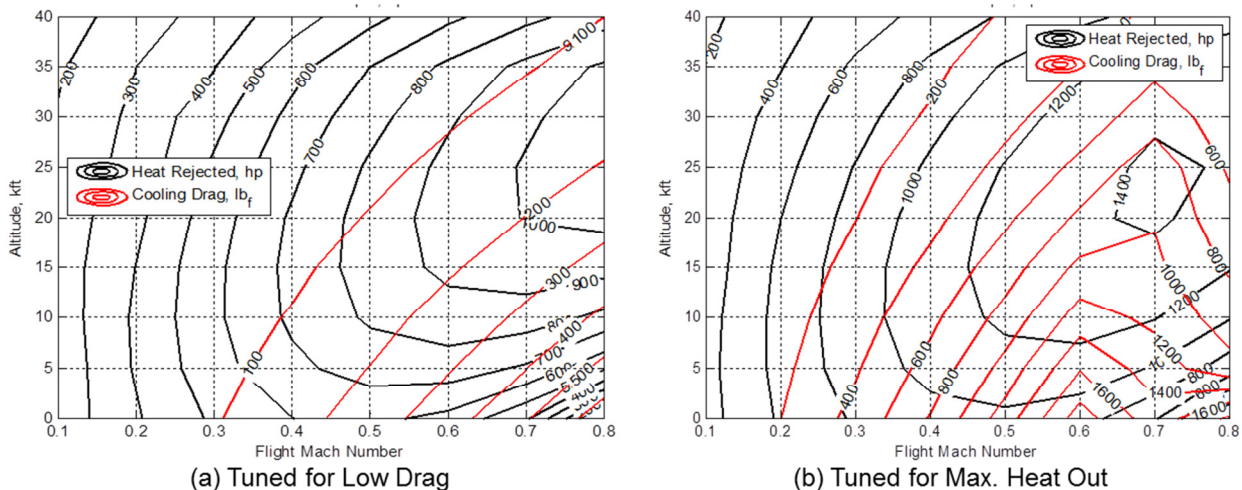


Figure 11. Ducted Radiator Off-design Performance.

Figure 11(b) shows the same radiator design tuned for maximum heat output. To accomplish this high heat output, the face Mach number was increased to the highest possible value for the operating condition. A bifurcation occurs between flight Mach 0.6 and 0.7 wherein the face Mach has reached the maximum allowable value; increasing the face Mach beyond that point would result in sonic flow within the duct. Regardless of nozzle tuning, the chosen design could not successfully reject all of the heat produced by the ECO-150R during the takeoff and OEI climbout conditions. A ducted radiator that could meet the high heat load at low airspeed conditions of takeoff and OEI climbout would need to be substantially larger, adding mass and cooling drag through the entire mission. Fortunately, both of these design conditions last for a very short amount of time during which a low grade thermal deficit could be tolerable. Although the average temperature of the coolant would steadily increase during these maneuvers, a system with enough thermal capacitance could safely complete the maneuver before the components overheat. Transient modeling of the TMS through a mission would be necessary to determine if the system could survive a takeoff to OEI climbout sequence without overheating.

The overall wet weight of the TMS including two ducted radiators, two pumps, and a simple network of coolant piping was found to be approximately 20% of the weight of the electronics that it cooled. This is an improvement over the 30% estimate that was used during previous design studies for “warm” ECO-150 variants; however, the cooling drag was not previously considered.

Despite the higher level of detail, the design and analysis of the thermal management system is far from complete. There are several opportunities for improvement of the design. For instance, the use of a variable area duct inlet could further reduce the drag of the system at different flight speeds at the expense of additional weight and complexity. Furthermore, the simple tube-and-fin heat exchanger configuration could be replaced by an optimally designed printed circuit heat exchanger. There are other design considerations, however, which could negatively impact the weight and drag of the design. For instance, it is likely that the network of coolant piping considered in the current design was too simplistic and needs to be revised to meet redundancy requirements.

IV. Propulsion-Airframe Integration Analysis

The tightly coupled propulsion-airframe integration has been a topic of considerable uncertainty for the ECO-150. The analysis presented in this section provides a baseline level of confidence in the aeropropulsive performance of the split-wing configuration while revealing possibilities for further improvement. Initial studies included high speed cruise and high lift, low speed scenarios. Furthermore, revisiting integration of propulsion, propulsion support, and structural components within the split-wing proved to be a valuable exercise for improved concept credibility and is also covered here.

A. CFD-Motivated Wing Reshaping

Much of the aerodynamic uncertainty surrounding the ECO-150 configuration centered on the split-wing concept occupying the inboard wing section. The propulsive and structural characteristics of the split-wing have been identified in previous efforts²; however, true understanding of the external flow behavior lacked, both in high and low speed scenarios. Estimation of lift and drag remained rudimentary, treating the split-wing as a typical airfoil which had been separated chord wise for embedded propulsion components and rounded to minimize flow separation. In order to capture and verify the analytical aerodynamic buildup conducted in early concept studies, a full 3D CFD study was performed. The motivation to conduct initial ECO-150R CFD studies was borne out of the results from an AFRL funded propulsion-airframe integration study by Lockheed Martin in which cruise aerodynamic improvements of 8% were found with inboard profile sections similar to that of the ECO-150 design⁵.

The ESAero team employed the NASA Langley Research Center (LaRC) Tetrahedral Unstructured Software System (TetruSS)²³ for its grid generation utilities and flow solver needs. TetruSS leverages VGRID²⁴ as its viscous, unstructured mesh generator. VGRID utilizes the Advancing-Layers²⁵ and Advancing-Front²⁶ Methods to create its final computational mesh composed of tetrahedra. This mesh is then used by the USM3D²⁷ flow solver. USM3D solves the full Navier-Stokes fluid equations including all cross terms with Reynolds-averaged Navier-Stokes formulation (RANS) including many 1- and 2-equation turbulence models in addition to a Detached-Eddy Simulation (DES) formulation. USM3D performs its parallel execution on multiple CPUs using zonal decomposition and Message Passing Interface (MPI)²⁸. To ensure the full capture of split-wing performance, proper bookkeeping of aerodynamic and propulsion boundaries took place.

Prior to configuration modifications, CFD results concluded that the existing inboard profile shape of the early ECO-150 concept exhibited a pronounced shock at the Mach 0.7 cruise condition. As shown in Figure 12, the leading edge curvature and excessively sloped lower surface induced shocks and unwarranted drag even at low angles-of-attack. The initial CFD results prompted a reshaping of the inboard profile to minimize drag while

maintaining adequate volume and spacing for component integration. Figure 13 shows the modified inboard profile and CFD results of surface coefficient of pressure. Iterations of the new airfoil geometry enabled the elimination of inboard wing shock at the cruise condition. The sweep of CFD analysis brought to light additional problem areas, such as the outboard wing section, which could be areas of further improvement for maximizing aerodynamic efficiency.

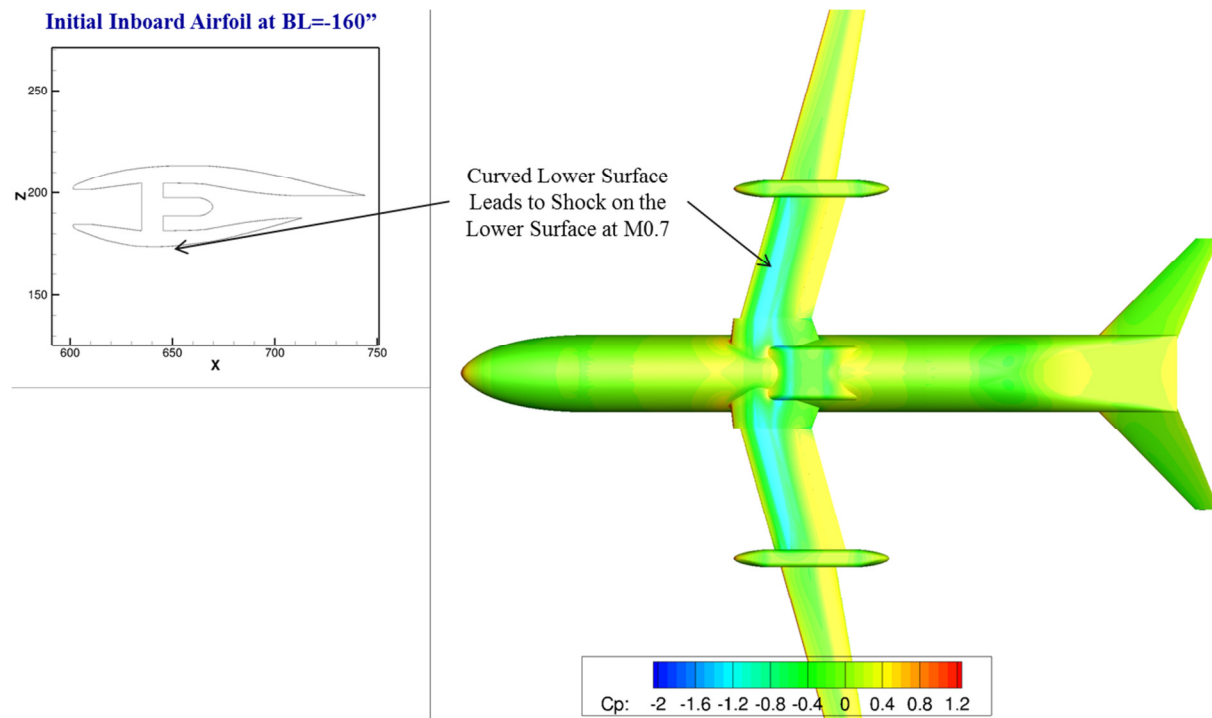


Figure 12. Initial CFD Results of Unmodified Inboard Profile

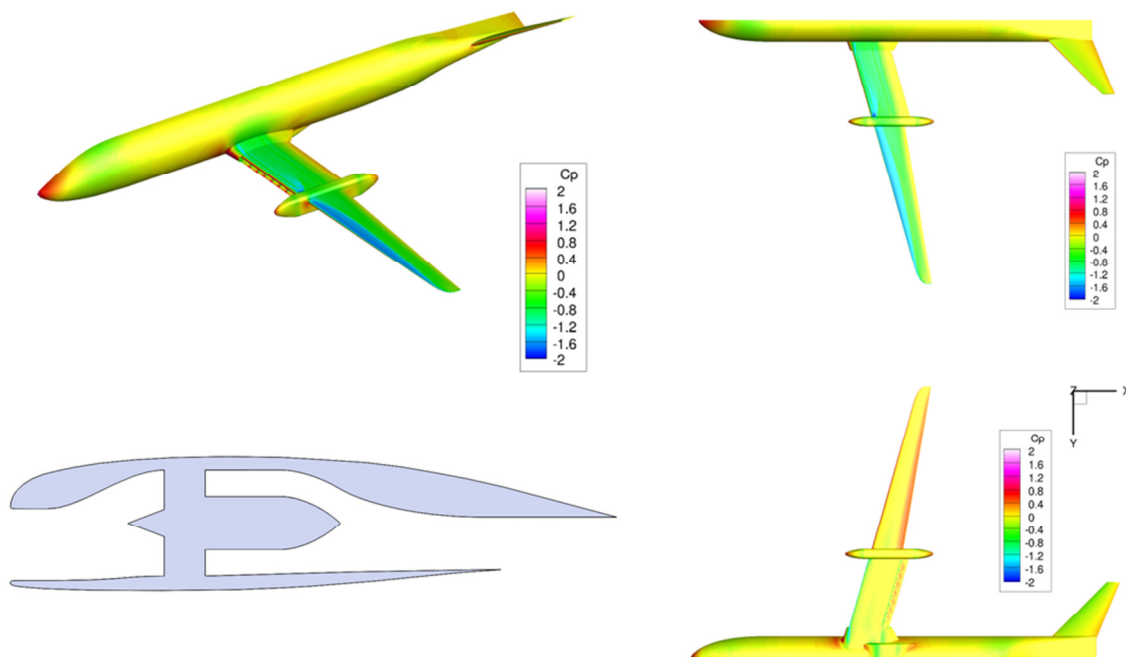


Figure 13. CFD Results of Modified Inboard Profile.

The intention of the investigative CFD study was to provide verification of the aerodynamic analysis on which the performance metrics were founded. Figure 14 shows the comparison between the previously determined analytical cruise drag polar and the CFD produced drag polar via alpha sweep at Mach 0.7 and 30,000 feet. The area of most interest is the region where cruise coefficient of lift (C_L) is between 0.4 and 0.7. Maximum lift-over-drag values of 18 at a C_L of 0.64 are achievable, thus indicating the inclusion of distributed propulsion need not come at an aerodynamic penalty. While CFD fails to capture drag producing items typically categorized as excrescence, several areas leave much room for improvement to initial results such as fuselage smoothing, wing fairing blending, outboard wing optimization, and landing gear pod improvements. As was stated in Ref. 5, embedded propulsion, referred to *split-wing* in the ECO-150 concept, yields at least similar aerodynamic efficiency to a standard podded configuration of similar power.

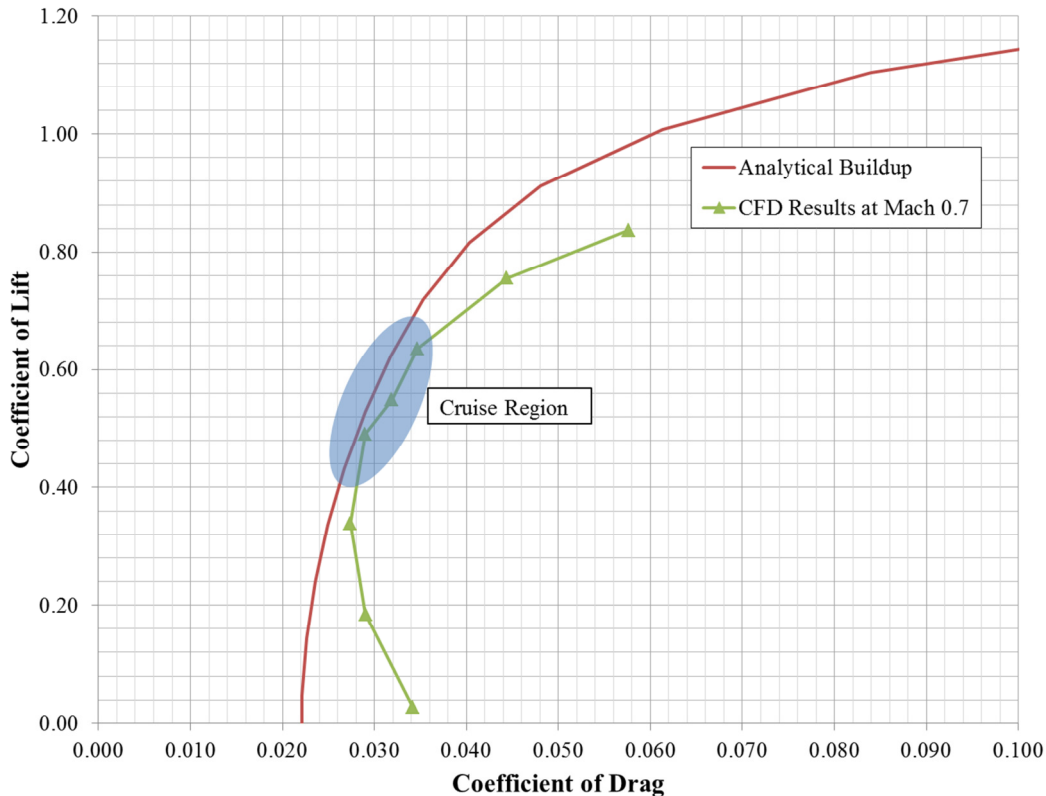


Figure 14. Analytical and CFD Drag Polar at M0.7 and 30,000 ft.

B. High Lift System

One of the major advantageous attributes to the split-wing distributed propulsion system is the ability to garner high coefficients of lift via powered-lift. The Quiet Short-haul Research Aircraft (QSRA)²⁹ and Boeing C-17³⁰ utilized deflected jet exhaust to increase circulation and improve C_L over an unpowered wing, enabling reduced takeoff and landing distances. The ECO-150 takes advantage of this effect by spreading the mass flow used for thrust span wise. A simple fowler flap was modeled and deflected at 40° to simulate a low speed approach configuration, as pictured in Figure 15.

Maintaining true to the propulsion system capability described in earlier sections, various flow conditions were set to mimic multiple power levels. An alpha sweep at sea level and Mach 0.2 was performed and analyzed using the CFD toolset formally outlined. Figure 16 showcases several 2D contour plots of coefficient of pressure (C_p) for

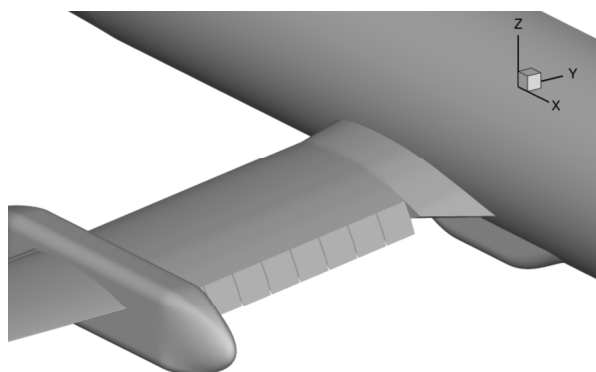


Figure 15. Simple Fowler Flap at 40° on the ECO-150R Inboard Wing Section.

various power settings. Maximum C_L ranged from just over 2.0 for unpowered to 2.6 with power set to 100%, yielding a significant powered-lift effect considering the simplicity of a short span, short chord, poorly integrated flap. Since the ECO-150R lacked a shorter than typical runway design requirement, standard C_L ranges can be achieved without the need for complex, heavy flap mechanisms.

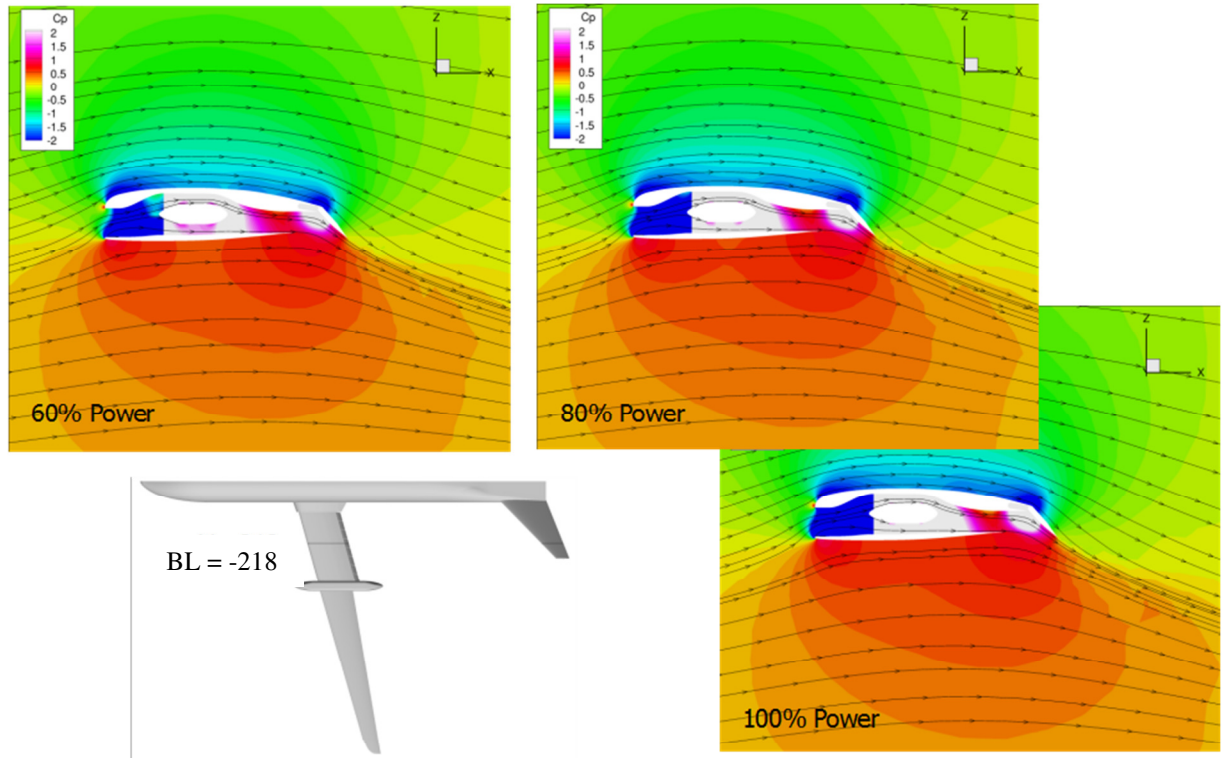


Figure 16. Coefficient of Pressure Plots of the Flapped ECO-150R Inboard Wing Section for Various Power Settings.

C. Component Integration

A major focus of the redesign effort was to apply 2-D and 3-D CFD analyses to the inboard wing to verify lift coefficient, drag coefficient, and transonic aerodynamics, the results of which are covered in the previous sections.

The first task was to change the geometry of the inboard wing to reflect CFD results. Figure 17 shows a first attempt to replicate the streamwise cross-section. Of immediate interest is the shorter chord and flattened lower surface. Fan diameter decreased slightly and motor length decreased dramatically due to revised sizing trends of the propulsion system components.

Earlier concept work sized the inboard wing structure and established a conceptual approach to layout that also fit nicely into the ECO-150R. Figure 18 shows this revised structural approach fitted into the center fuselage structure to align major load paths. Existing bulkheads and frames moved slightly but no new structure was needed. Figure 18 also depicts isometric views of the partially completed inboard wing solid model. Upper and lower forward spars were placed to support the fan bay inlets and to provide sufficient rigidity to hinge upper and/or lower

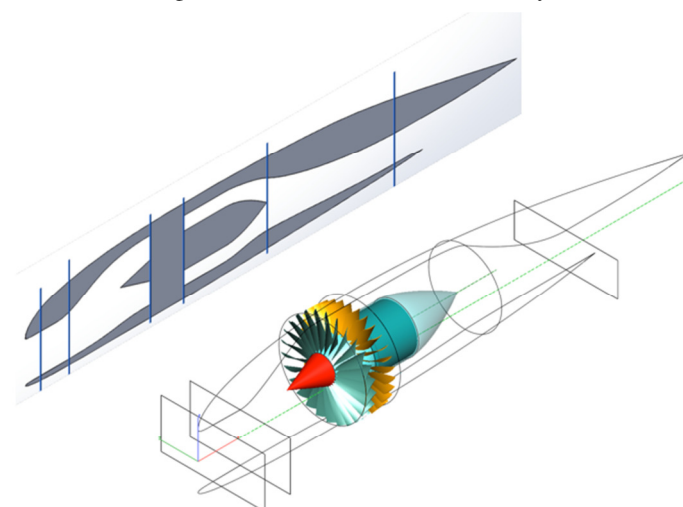


Figure 17. Integrated Motor and Fan within Redesigned Inboard Profile.

leading edges either for high lift or to control airflow into the fan ducts. Upper and lower aft spars were placed to provide rigidity for lower surface flaps as well. Upper surface flap tracks could be cantilevered off the upper spar as well. Again, rotating the movable surfaces would provide both high lift and exit airflow control.

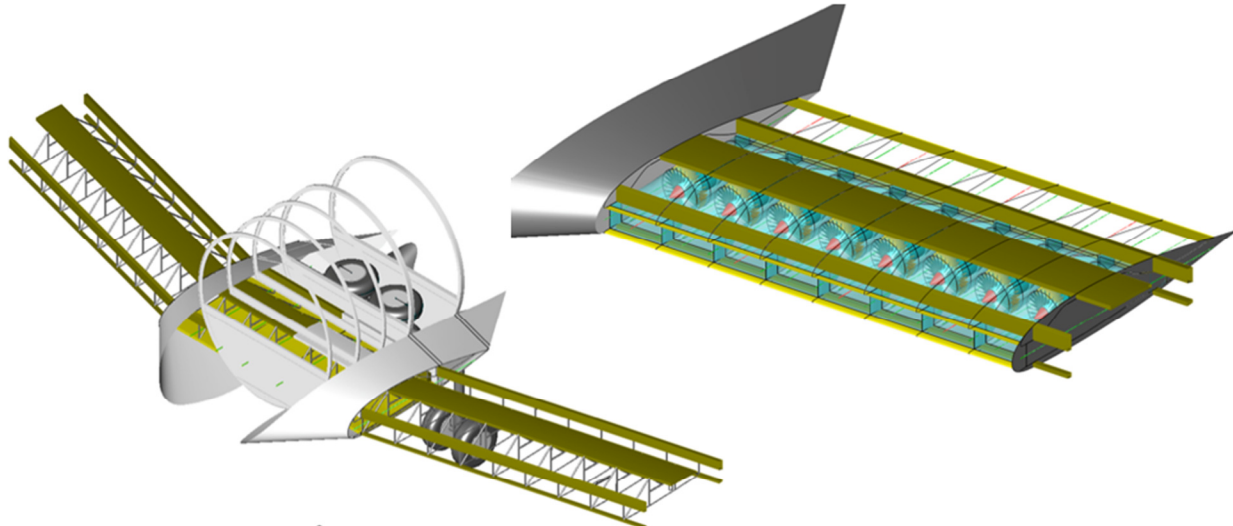


Figure 18. ECO-150R Inboard Wing Structure and Fitted Propulsion System.

The power train components discussed in Section II were also integrated into the configuration. Figure 19 presents an isometric view of a simplified solid model showing just the power train components that require either coolant or electrical cabling. Note that each nacelle contains two clutched generators per turboshaft engine. Coolant line diameters and electrical cable diameters are to scale as specified by the power train design team. While the electrical cables are just over an inch in diameter, the multitude of runs rapidly fill up the upper surface torque box. Placing the electrical cables so they did not interfere with coolant lines and structure while aligning as close as possible with the components they run to required several iterations.

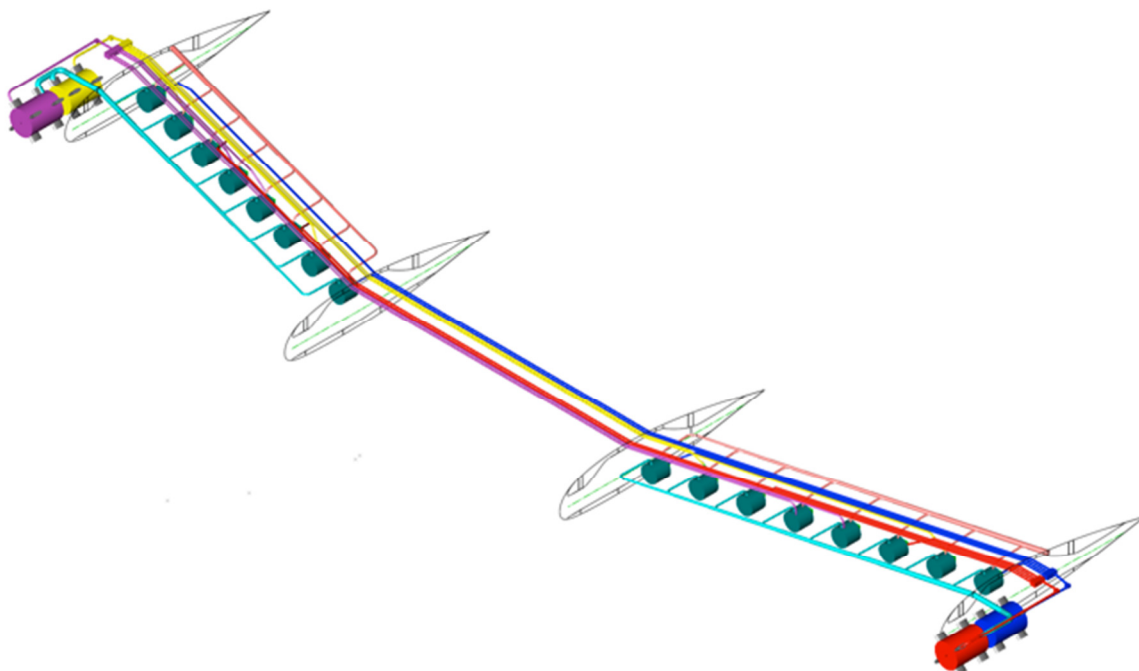


Figure 19. Simplified Solid Model Isometric View of Motors, Generators, Coolant, and Electric Cable Runs.

Figure 20 showcases the details of the newly sized ducted radiator system and propulsion components. The turboshaft engine decreased slightly in diameter and length but still fit nicely into the original ECO-150-16 nacelle. Integration of necessary pumps, junction boxes, piping turns, and reservoirs showed that the original nacelle was just

too small in cross-section, so the nacelle cross-section was iterated as internal power train components were laid out. Note in Figure 20 that two major nacelle bulkheads align with forward and aft inboard wing spars to provide load continuity across the nacelle. There are also frames at the radiator inlet and around the aft turboshaft engine mount (shown in tan). The forward engine mounts (also shown in tan) are aligned with the nacelle frame at the aft inboard wing spar. Horizontal structural beams provide a keel of sorts and allow rotating components and the heat exchanger to be raised or lowered through the nacelle bottom for service or replacement. The inboard wing upper surface torque box provides dedicated space to house electrical runs, splitters, and junction boxes; it and the outboard side beam provide load support for the high aspect ratio outboard wing panel.

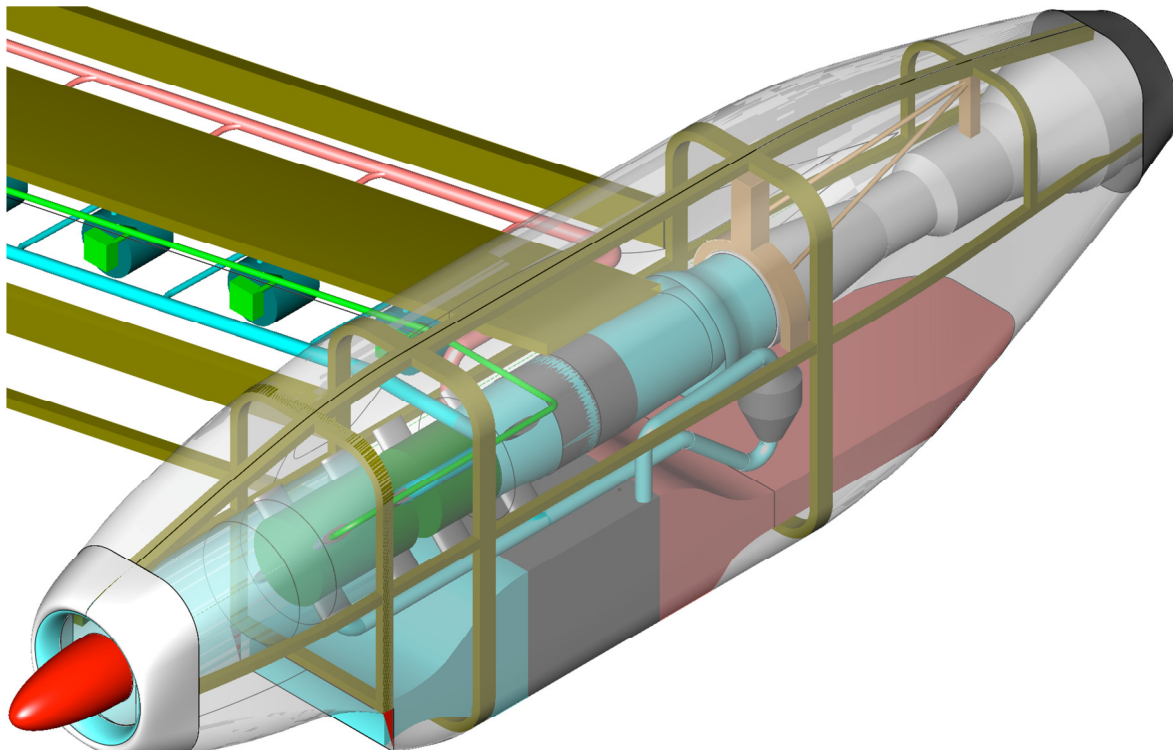


Figure 20. Turboelectric Nacelle Internal Details.

V. Performance and Mission Analysis

An off-design analysis mode of PANTHER was developed to capture much of the complex operating condition interactions, efficiency maps, and component-specific performance limits and generate a consolidated “engine map” for the ECO-150R. This algorithm utilizes a constrained optimizer to respect performance limits and establish TSFC trends throughout a range of throttle settings and at all flight conditions. The maximum thrust available and associated TSFC of the propulsion system are shown in Figure 21. Markers indicate cases in which the engine power code (PC), or percent of power available used, had to be reduced from 100% due to limitations of other propulsion system components such as motors and generators.

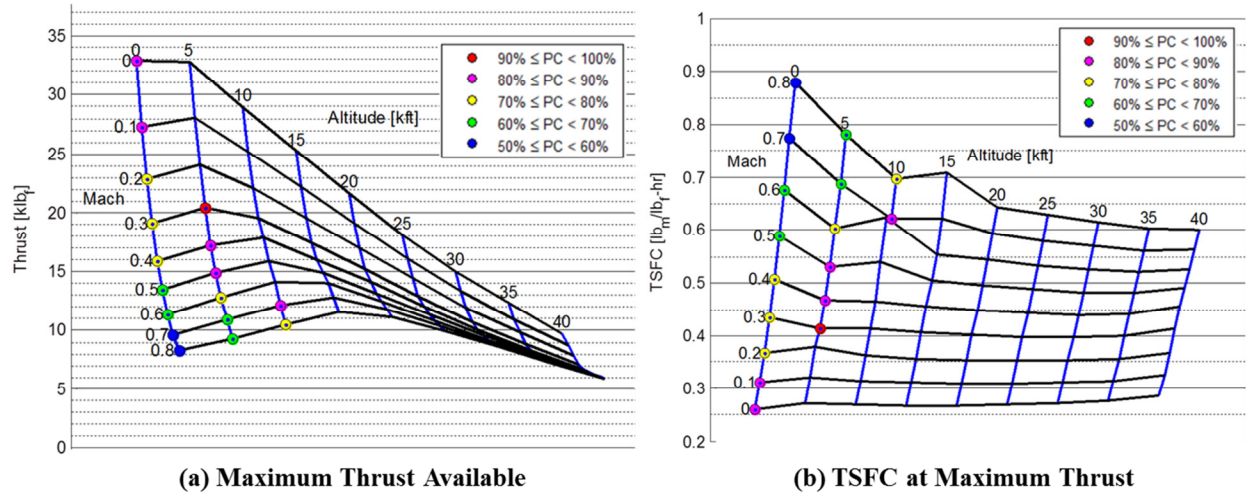


Figure 21. ECO-150R Off-Design Performance Maps.

In addition, a CFD study was performed to gain a better understanding of inboard aerodynamic behavior and overall aircraft drag. The results from the CFD study were compared to the analytical drag buildup showing close agreement of the drag polars throughout the cruise region (where a majority of the mission takes place); differences between the CFD analysis and the analytical drag buildup can be attributed to the differing levels of detail between the two. The comparison concluded that an ML/D of 13 at the beginning of cruise is easily obtainable.

Mission analysis was then performed, where the mission setup remained consistent with previous studies for proper comparison. In comparison with several Boeing 737 arrangements (See Figure 22 and Figure 23), the ECO-150R continues to show great promise with a payload range of 1,646 n.mi (designed maximum payload range was

1,500 n.mi) and an efficiency comparable to the 737-700 with 68 seat-miles per gallon.

Further iterations on this vehicle will surely improve the seat-miles per gallon. While the CFD and drag buildup analysis confirms an aerodynamic transport efficiency of 13, the 1-g transport efficiency at the beginning of cruise was determined to be less than 11 due to the reduction in takeoff gross weight. This forces the aircraft to fly at a non-optimal lift coefficient. In other words, the wing in its current state is too large with a wing loading of around 80 pounds per square foot (psf) as opposed to the designed 100 psf. Not only will fuel burn be reduced,

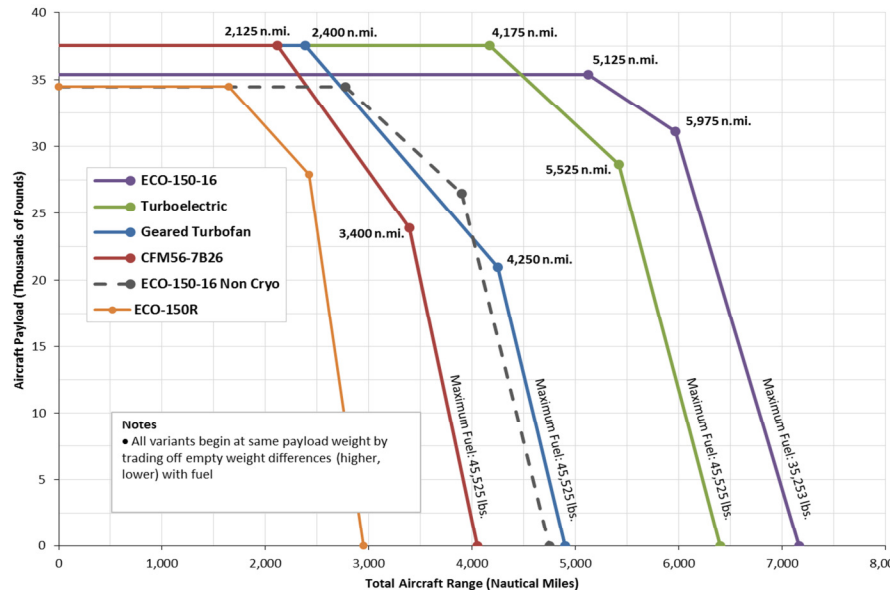


Figure 22. Payload-Range Comparison.

further reduction in structure weight and aerodynamic drag will significantly improve overall fuel efficiency.

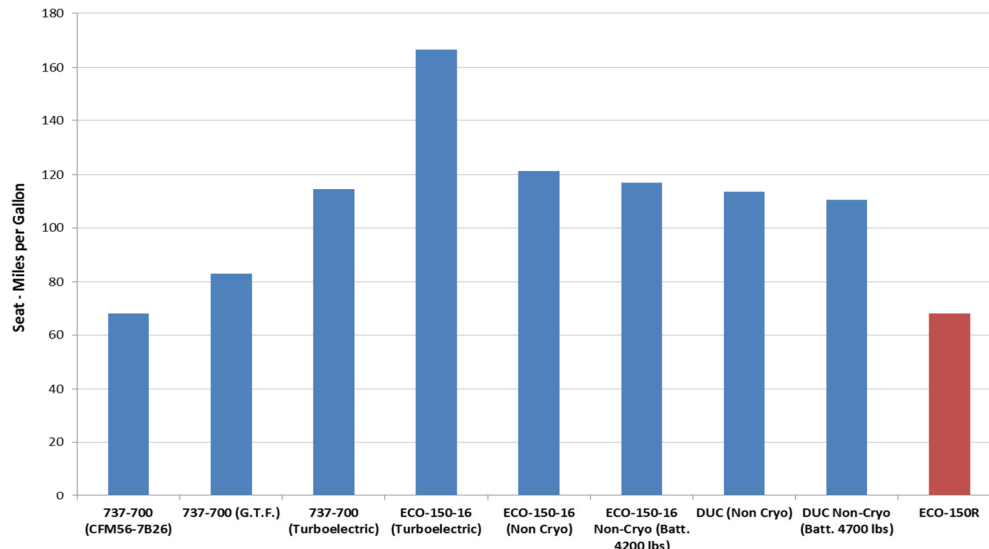


Figure 23. Seat-miles per gallon for Fuel Comparison.

VI. Conclusion

When ESAero undertook initial ECO-150 and ECO-250 studies in 2009, prevailing opinion in the industry (and at ESAero) was that tube and wing configurations might not be efficient enough to benefit from integrated propulsion schemes such as turboelectric distributed propulsion encased in a split-wing. That assumption has proven to be conservative if the studies described in this paper turn out after full-scale flight demonstration to have merit. Results to date are certainly promising enough to warrant building physical subscale models and bench testing them, testing them in wind tunnels, and eventually flight testing them using existing aircraft in the NASA or military fleets. These tests will be exciting in their implication of achieving NASA's 2004 goal of markedly reducing fuel consumption, emissions, and noise of future civilian and military fleets.



Acknowledgments

Empirical Systems Aerospace, Inc. would like to thank Dr. Michael Armstrong of Rolls-Royce Liberty Works, Darold B. Cummings of ESAero, and the Helden Aerospace consulting team.

References

- ¹Empirical Systems Aerospace, Inc., "Integration of an Advanced Cryogenic Electric Propulsion System (ACEPS) to Aerodynamically Efficient Subsonic Transport Aircraft," NASA SBIR Phase I Final Report, Contract No. NNX09CC86P, 2009.
- ²Empirical Systems Aerospace, Inc., "The Design and Integration of a Distributed Fan Propulsion System within a Split-Wing," NASA SBIR Phase I Final Report, Contract No. NNX10CC81P, 2010.
- ³Schiltgen, B., et al., "Benefits and Concerns of Hybrid Electric Distributed Propulsion with Conventional Electric Machines," AIAA 2012-3769, 48th AIAA/ASME/SAE/ASEE Joint Propulsion Conference & Exhibit, Atlanta, GA, August 2012.

- ⁴Empirical Systems Aerospace, Inc., "Cryogenic and Non-Cryogenic Hybrid Electric Distributed Propulsion with Integration of Airframe and Thermal Systems to Analyze Technology Influence," NASA SBIR Phase I Final Report, Contract No. NNX15CD15P, 2015.
- ⁵Wick, A. T., Hooker, J. R., Hardin, C. J., and Zeune, C. H., "Integrated Aerodynamic Benefits of Distributed Propulsion," AIAA 2015-1500, 53rd AIAA Aerospace Sciences Meeting, AIAA SciTech, 2015.
- ⁶Empirical Systems Aerospace, Inc., "Hybrid-Electric Aircraft TOGW Development Tool with Empirically Based Airframe and Physics Based Hybrid Propulsion System Component Analysis," NASA SBIR Phase I Final Report, Contract No. NNX13CC24P, 2013.
- ⁷Empirical Systems Aerospace, Inc., "Physics-Based Radiator Design, Sizing, & Weight Estimation Tool for Conceptual Design of More-, Hybrid-, and All-Electric Next Gen Aircraft," NASA SBIR Phase I Final Report, Contract No. NNX14CC57P, 2014.
- ⁸Empirical Systems Aerospace, Inc., "Hybrid-Electric and All-Electric Rotorcraft Analysis and Tool Development," NASA SBIR Phase I Final Report, Contract No. NNX14CA27P, 2014.
- ⁹Green, M., Schiltgen, B., Gibson, A., "Analysis of a Distributed Hybrid Propulsion System with Conventional Electric Machines," AIAA 2012-3768, 48th AIAA/ASME/SAE/ASEE Joint Propulsion Conference & Exhibit, Atlanta, GA, August 2012.
- ¹⁰Green, M., "HAPSS, Hybrid Aircraft Propulsion System Synthesis," M.S. Thesis, Aerospace Engineering Dept., California Polytechnic State Univ., San Luis Obispo, CA, 2012.
- ¹¹Roskam, J., *Airplane Design, Part I: Preliminary Sizing of Airplanes*, DARcorporation, Lawrence, KS, 1997, pp. 154.
- ¹²Anderson, J. D. Jr., *Aircraft Performance and Design*, WCB/McGraw-Hill, Boston, 1999, pp. 272, 412-413.
- ¹³Armstrong, M., et al., "Architecture, Voltage, and Components for a TurboElectric Distributed Propulsion Electric Grid Final Report," NASA/CR—2015-218440, 2015.
- ¹⁴Winter, M., "A View into the Next Generation of Commercial Aviation (2025 Timeframe)," AIAA Aerospace Today & Tomorrow, 2013.
- ¹⁵Alyanak, Edward J. and Allison, Darcy L., "Fuel Thermal Management System Considerations in the Aircraft Conceptual Design Process," AIAA 2016-0670, 57th AIAA/ASCE/AHS/ASC Structures, Structural Dynamics, and Materials Conference, AIAA SciTech, January 2016.
- ¹⁶Meredith, F. W., "Note on the cooling of aircraft engines with special references to ethylene glycol radiators enclosed in ducts", British ARC, Reports and Memoranda No. 1683, London, England, 1935.
- ¹⁷Bergman, T. L., Lavine, A. S., Incropera, F. P., and Dewitt, D. P., *Introduction to Heat Transfer*, 6th ed., John Wiley and Sons, Inc., Jefferson City, MO, 2011.
- ¹⁸Shah, Ramesh. K. and Sekulić, Dušan. P., *Fundamentals of Heat Exchanger Design*, Wiley India Pvt, 2013.
- ¹⁹Crosthwait, E. L., Kennow, I. G., and Roland, H. L., "Preliminary Design Methodology for Air-Induction Systems," Systems Engineering Group Research and Technology Division Air Force Systems Command, Rept. SEG-TR-67-1, Wright-Patterson Air Force Base, 1967.
- ²⁰Henry, J. R., Wood, C. C., and Wilbur, S. W., "Summary of Subsonic-Diffuser Data," NACA-RM-L56F05, 1956.
- ²¹Mattingly, J. D., Heiser, W. H., and Pratt, D. T., *Aircraft Engine Design*, 2nd ed., AIAA Education Series, Reston, VA, 2002 (pages 192-193).
- ²²John, James E. and Keith, Theo G., *Gas Dynamics*, 3rd ed., Pearson Education, Inc., Upper Saddle River, New Jersey, 2006.
- ²³Frink, N.T., Pirzadeh, S.Z., Parikh, P.C., Pandya, M.J., and Bhat, M.K., "The NASA Tetrahedral Unstructured Software System," The Aeronautical Journal, Vol. 104, No. 1040, October 2000, pp. 491-499.
- ²⁴Kania, L. and Pirzadeh, S. Z., "A Geometrically-Derived Background Function for Automated Unstructured Mesh Generation," AIAA 2005-5240, 17th AIAA Computational Fluid Dynamics Conference, Toronto, Ontario, Canada, June 2005.
- ²⁵Pirzadeh, S.: "Unstructured Viscous Grid Generation by Advancing-Layers Method," AIAA 93-3453, August, 1993. Also, AIAA Journal, Vol. 32, No. 8, August 1994, pp. 1735-1737.
- ²⁶Pirzadeh, S., "Three-Dimensional Unstructured Viscous Grids by the Advancing Front Method," AIAA Journal, Vol. 34, No. 1, January 1996, pp. 43-49.
- ²⁷Pandya, M.J., Abdol-Hamid, K.S., Campbell, R.L., and Frink, N.T., "Implementation of Flow Tripping Capability in the USM3D Unstructured Flow Solver," AIAA 2006-0919, 44th AIAA Aerospace Sciences Meeting and Exhibit, Reno, NV, Jan. 2006.
- ²⁸MPI Forum, "MPI Documents," URL: <http://www.mpi-forum.org/docs/docs.html> [cited 13 December 2015].
- ²⁹Shovlin, M. D., and Cochrane, J. A., "An Overview of the Quiet Short-Haul Research Aircraft Program," NASA-TM-78545, 1978.
- ³⁰NASA, "NASA Contributions to the C-17 Globemaster III," NASA Factsheet No. FS-1996-05-06-LaRC, May 1996.